



Applying a realistic novel ventilation model based on spatial expansion of acini in a stochastic lung

R. Dastanpour^a, M. Monjezi^a, M.S. Saidi^{b,*} and A. Pishevar^a

a. *Department of Mechanical Engineering, Isfahan University of Technology, Isfahan, Iran.*

b. *School of Mechanical Engineering, Sharif University of Technology, Tehran, Iran.*

Received 6 August 2012; received in revised form 22 July 2013; accepted 3 February 2014

KEYWORDS

Spatial ventilation model;
Acini expansion;
Stochastic whole lung;
Monte Carlo modeling;
Particle deposition.

Abstract. In this paper, particle deposition in the upper airways and five lobes of a human lung is simulated. The simulation is based on a stochastic lung model, derived from detailed morphometric measurements. Pathways are simulated using Monte Carlo methods; consequently the whole structure changes both stochastically and statistically in each simulation. In this investigation the termination phenomena is a function of each daughter's diameter which best satisfies the lung's morphometry. Complementary to the previous available assumptions, i.e. flow divisions according to the ratio of daughter's cross sections or distal volumes, in this investigation flow rates are computed in an upward manner starting from the acini (where suction occurs), following to trachea. Regional expansion and contraction coefficients of acinar airways are taken into account in the airflow distribution analysis. Regional and total deposition fractions in the human respiratory system are computed by astochastic lung deposition model in a full breathing cycle. These fractions are computed in the upper airways as well as the above mentioned stochastic lung instead of a pre-defined lung structure. The effects of Brownian motion, inertial impaction and gravitational sedimentation are simulated in particle deposition analysis in respiratory airways using analytical equations.

© 2014 Sharif University of Technology. All rights reserved.

1. Introduction

Many models have been described in literature for simulating lung airways structure. Weibel [1] developed the simplest model of the lung airways network which is completely planar and symmetrical. Opposite to this simple model, Raabe et al. [2] and Horsfield et al. [3] provided partial and completely asymmetric models respectively. These models represent pre-specified geometries for human lung, such as diameter, length, number of airways, branching and gravity angles. The statistical nature of the morphometry of the tracheobronchial tree has been analyzed by

Koblinger and Hofmann [4]. They have provided a set of statistical distributions of the parameters used in determination of the lung's airways structure. They also have derived an algorithm to create a series of single paths using their statistical distributions. In addition to the improvements made on some steps of their algorithm in this study, new steps are added to create a new algorithm constructing "whole lung" airways based on Monte Carlo methods.

Realistic models describing lung structure and airflow distribution are the determinant factors in the estimation of particle deposition in respiratory system. Although many researchers have focused on the models describing lung airway's geometry, little efforts are devoted to the realistic simulation of airflow distribution in respiratory airways. Contrary to an idealized symmetric lung model, respiration airflow

*. *Corresponding author. Tel.: +98 21 66165558;
Fax: +98 21 66000021
E-mail address: mssaidi@sharif.edu (M.S. Saidi)*

cannot be divided uniformly among the airways in an asymmetric whole lung. Many models have been developed for estimating airflow distribution in lung airways. Examples of these models are empirical ventilation models which are based on specified airway structures and cannot be applied in different geometries, models that assume each daughter's airflow share of its parent to be proportional to the ratio of daughter's cross sections [5,6] and models in which distal volumes are utilized for calculating each airway's share of the inhaled air [7].

According to the physiology of respiration [8,9], air suction during inspiration is caused by the expansion of the alveolated pathways. On the other hand, during inhalation, diaphragm muscle moves downward, chest volume increases and the pleural pressure falls down. As a result, air sacs start spreading out and environmental air gets through the lung pathways.

In this study flow rates in airways are computed in an upward manner starting from the acini (where suction occurs), following to trachea. Contrary to the models in which distal volumes are utilized in calculation of airflow distribution in lung airways regardless to the actual number of the pulmonary airways connected to each airway [7], in current model total number and expansion coefficients of pulmonary airways which are connected to each airway's ongoing-generations are utilized in airflow simulations. To this end, regional expansion coefficients of acinar packs are derived based on the spatial location of airways and applied in our calculations in order to estimate flow rates more accurately. The airflow distribution results are compared to the previous available assumptions, i.e. flow divisions according to daughter airway dimensions [5,6].

Many researchers have also analyzed particle deposition in human lung airways. Even though they have simulated deposition in a sample bifurcation [10,11] through a set of bifurcations [12], or in a symmetric lung [13], but little efforts are devoted to the modeling of particle deposition in a whole asymmetric, un-predefined lung.

Regional and total particles deposition fractions are also estimated in upper airways and the whole airways of the simulated lung's five lobes in a complete breathing cycle.

2. Model description and numerical strategy

In order to simulate particle tracking and deposition in human respiratory system, three main steps should be followed. First, accurate and realistic lung geometry should be defined. To this end, stochastic variation of the fundamental geometrical parameters, e.g. diameter and length, should be considered. Procedures used in this study to simulate lung airways are described in more details in Section 3.

Next step is to develop a model for flow distribution characterization among lung airways. Complementary to the previous models, i.e. flow divisions according to the ratio of daughters' cross sections or distal volumes, in this investigation flow rates are computed in an upward manner starting from the acini (where suction occurs), following to trachea. This leads to a more realistic model and more accurate regional flow distribution and particle deposition estimations. This step is described in Section 4.

Final step is to simulate particle deposition in the simulated lung airways. To this end, analytical equations are used to estimate particle deposition in simulated lung structure. This step is described in more details in Section 5.

3. Lung geometry

3.1. Tracheobronchial tree airways structure

Human lung is modeled by a sequence of tubes branching into two daughter airways. Diameter, length, branching and gravity angles are the design parameters of the lung pathways which have to be determined.

Koblinger and Hofmann [4] have provided statistical distributions for 6th-21th generation numbers of lung airways. Consequently, actual measured airway dimensions (length, diameter, branch angle and gravity angle) are used [2] for the first five airway generations in our lung model.

In this study both daughters which branch in each bifurcation are taken into account and their geometrical parameters as well as their connection links to former and latter airways are stored and utilized.

The method used in this study in determination of each geometrical parameter of the lung airways is discussed in the proceeding sections.

3.1.1. Diameters of tracheobronchial tree airways

The distributions of the cross section ratios and the diameter ratios of the minor and major tubes of the same parent are reported by Koblinger and Hofmann [4]. Corresponding ratios of these parameters (f_1 and f_2) are selected by comparing randomly generated numbers with cumulative probability distributions of these parameters. Minor and major daughters' diameters (d_i and d_i^*) are determined by solving the following Equations:

$$d_{i^*} = \sqrt{\frac{d_{i-1,j}^2}{f_1(1+f_2^2)}}, \quad (1)$$

$$d_i = f_2 d_{i^*}. \quad (2)$$

3.1.2. Lengths of tracheobronchial tree airways

Koblinger and Hofmann [4] presented the averages and the relative standard deviations of the logarithms

of lengths and diameters. They also reported 7 frequency distributions relating lengths classes to diameters classes. In order to utilize these data for determination of pathway's lengths, the probability distribution functions of the logarithms of diameters and lengths are calculated for each generation number. These distribution functions are determined using Eq. (3).

$$y = f(x, \mu, \sigma) = \frac{1}{x\sigma\sqrt{2\pi}} e^{-\frac{(\ln x - \mu)^2}{2\sigma^2}}, \quad (3)$$

where y is the corresponding value, e.g. diameter or probability for the log-normal distributed parameter, x is the log-normal distributed parameter, σ is the standard deviation, and μ is the average logarithm of x .

In order to make a discrete distribution for the diameter and lengths of the tubes, each probability distribution function of the logarithms of tube diameters and lengths is tallied into seven equal-probability classes. Using this method, seven diameter size bins and seven length size bins are produced.

Subsequently, the following scheme was used for determination of the tubes lengths:

1. d_j , diameter of the pathway which has already been estimated by the procedure described in Section 3.1.1, is compared with the i th generation's diameter classes intervals to determine the corresponding diameter class number, N_d .
2. According to the value of N_d , the corresponding frequency distribution is selected from the 7 frequency distributions provided by Koblinger and Hofmann [4]. Afterward length class N_l is determined applying Monte Carlo method to the selected distribution.
3. The daughter's length is equal to the average of the lengths of N_l intervals.

3.1.3. Branching and gravity angles of tracheobronchial tree airways

In each generation, minor and major branching angles can be determined by applying Monte Carlo methods on the probability distributions provided by Koblinger and Hofmann [4].

Unfortunately, available data on gravity angles are less than satisfactory for reliable statistical evaluation. Consequently, values reported by Yeh and Schum [14] are applied in our model.

3.1.4. Termination in tracheobronchial tree

For three reasons the termination correlation reported by Koblinger and Hofmann [4] is not applied in our model:

- i) They assumed linear decrease in diameters and lengths of the pathway. However it could be altered using latest models [15].

- ii) In their model the termination is checked for the parent tubes therefore there are only two cases available. i) None of the daughters is alveolated; ii) Both of the daughters are alveolated. However in reality each of the daughters which branch in each bifurcation could be alveolated or non-alveolated independently.
- iii) The acinar model applied in current simulation could not be matched with that model. As a result the termination probability was changed to the following correlation: If $d_l \leq 0.5$ mm the l th branch is terminated and is the first alveolated path of its connected acinar pathways.

3.1.5. Spatial location of the airways

As mentioned, in this study whole lung structure is simulated statistically. As a result each duct's spatial coordinates could be calculated. For this purpose, cumulative branching angles (sum of the branching angles of the ducts leading to each pathway, starting from trachea) are used. The branching angles and gravity angles of the minor and major daughters are assumed to have positive and negative values, respectively. Spatial coordinates of the end of each pathway could be determined using Correlations (4)-(6):

$$x^* = x_p + l_p \cos(\varphi^*) \sin(\theta_p^{\text{cum}}), \quad (4)$$

$$y^* = y_p - l_p \cos(\varphi^*) \sin(\theta_p^{\text{cum}}), \quad (5)$$

$$z^* = z_p + l_p \sin(\varphi^*), \quad (6)$$

where *, p and cum indices are used for daughter branch, parent tube and cumulative parameters, respectively. l , φ and θ also represent the values of length, gravity angle and branching angle, respectively. The origin of the coordinate system used in this study is located at trachea's entrance (Figure 1).

3.2. Acinar airways structure

Contrary to the linear model of Koblinger and Hofmann [16], the idealized typical model of the pulmonary airways given by Weibel et al. [15] is utilized in the present work (Table 1).

The diameter of the first generation of acinar pathways in this model is assumed to be 0.5 mm, which is used in the termination correlation (Section 3.1.4).

4. Airflow distribution in lung airways

In order to prepare a realistic airflow distribution in lung airways, an upward computation is used. It starts from acini and follows to trachea. In this study inhaled air distributes between acinar packs. So as to calculate airflow distribution more accurately, we utilized regional "airflow share coefficients" of acinar packs. According to Des Jardins [8] and West [9]

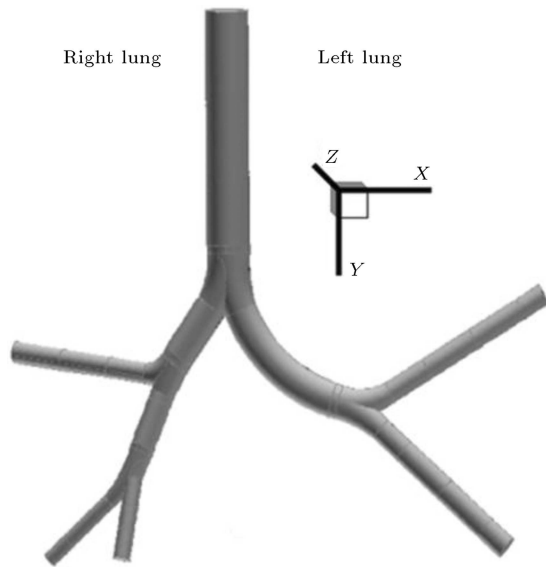


Figure 1. Orientation of the coordinate system used in this study.

Table 1. Idealized typical path model of acinar airways (Weibel et al. [15]).

Gen.	Segments		
	z'	$N(z')^a$	$l(\text{mm})^b$ $d_{in}(\text{mm})^c$
0	1	1.4	0.50
1	2	1.33	0.50
2	4	1.12	0.49
3	8	0.93	0.40
4	16	0.83	0.38
5	32	0.70	0.36
6	64	0.70	0.34
7	128	0.70	0.31
8	256	0.70	0.29

^a: $N(z')$: number of branches per generation;

^b: l mean length; ^c: d_{in} mean inner diameter of segments.

acinar airways do not expand uniformly in the lung. They reported that pulmonary airways' airflow share coefficient is a function of their location in the chest. We utilized the regional distribution curve of the pressure and volume of pulmonary airways reported in West [9] (Figure 2). In this study, this distribution is estimated by the Correlation (7):

Airflow share coefficient = 0.2

$$+0.8 \sin\left(\frac{\pi}{2} \times \frac{y_p - y_{\min}^{\text{lung}}}{y_{\max}^{\text{lung}} - y_{\min}^{\text{lung}}}\right), \quad (7)$$

where y_p is the coordinate of the acinar pack's entrance (y axis is illustrated in Figure 1) and y_{\min}^{lung} and y_{\max}^{lung} are the minimum and maximum of the coordinates of the bronchial tree airways, respectively.

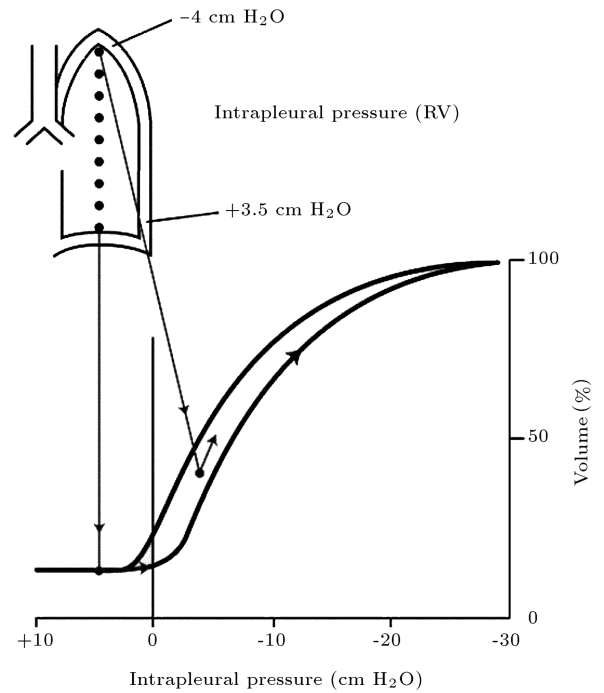


Figure 2. Regional distribution curve of the pressure and volume of pulmonary airways [9].

According to this correlation, acinar packs intake different airflows based on their spatial location. Each acinar pack has an airflow share coefficient ranging from 0.2 to 1.0. In current model, inspiration flux (500 cc) is divided among acinar packs according to these airflow share coefficients.

In order to consider the morphometry of the human lung, the following algorithm is used:

- (1) Calculate the sum of the airflow share coefficients belonging to each pathway;
- (2) Calculate the sum of the airflow share coefficients in the whole lung;
- (3) Calculate each duct's share of the total inhaled airflow. This share is equal to the ratio of the total sum of the airflow share coefficients connected to each tube to the sum of the airflow share coefficients in the whole lung;
- (4) Multiply values computed in the previous step by total inhalation airflow.

For example, if the whole lung consists of 31000 acinar packs and inhalation airflow is 500 cc per breathing cycle, each acinar pack will intake 3.2 – 16.0 mcc air based on its spatial location.

5. Deposition patterns

Inhaled particles penetrate deeper and deeper into the lung airways during inspiration and they should be followed continuously. The total number of airways

which should be taken into account in the “whole lung” modeling is enormously large. The “whole lung” modeled in our study consists of an average number of 45000 tracheobronchial tree tubes and about 14 million alveolated pathways. As a result of the high computational costs needed for CFD analysis of airflow and particle tracking in such a large structure, deposition is not simulated directly in our model. For the sake of improving the statistics of the Monte Carlo computations, the statistical weight method is applied. This means that a unit weight is assigned to each particle entering the human’s respiratory system. While particles move in lung airways, their statistical weights decrease. In the current study, three cases of oral breaching, nasal breathing and breathing directly from the trachea are considered. The statistical weight is followed in the pathways in an inward manner. To this end, deposition probability is calculated in each pathway. Then, the deposited fraction of particles in each pathway is computed by the product of its entering statistical weight and the calculated deposition probability. At each bifurcation, the statistical weight of the particles leaving the parent airway is segregated between daughters in a portion of their flux shares.

This downward procedure may be stopped for two reasons: i) When the statistical weight becomes significantly small and falls below a predefined threshold (in fact, the probability of deposition can never become zero; it can only become infinitesimally small), and ii) When inhalation time expires.

This process is also applied during exhalation in an upward manner providing input for oral and nasal cavity deposition predictions.

In the present work, basic deposition mechanisms, namely impaction, sedimentation and diffusion, are taken into account during inhalation, excluding the alveoli in the alveolated zone where velocities are very low. Impaction is also neglected during exhalation.

5.1. Deposition in nasal cavity

Deposition probability in the nasal cavity during inspiration uses the approach of Shi et al. [17].

$$DP_{\text{nasal}}^{\text{in}} = 1 - \exp(a \cdot \text{IP}), \quad (8)$$

where $a = 4.61 \times 10^{-5}$, $\text{IP} = d_a^2 \cdot Q$, d_a is the particle aerodynamic diameter and Q is volumetric airflow rate.

However, since no data was provided for exhalation, the correlation reported by Stahlhofen et al. [18] was used for exhalation.

$$DP_{\text{nasal}}^{\text{ex}} = 0.033 + 0.003 \log(\text{IP} \times 10^{18})$$

$$\text{if } \text{IP} \times 10^{18} \leq 215,$$

$$DP_{\text{nasal}}^{\text{ex}} = -0.815 + 0.399 \log(\text{IP} \times 10^{18})$$

$$\text{if } \text{IP} \times 10^{18} > 215. \quad (9)$$

5.2. Deposition in oral cavity

Particle transport and deposition results reported by Zhang et al. [19] are used for deposition calculations in a human’s oral cavity during inspiration. The deposition fraction vs. Impaction Parameter (IP) curve reported in their work can be estimated by Eq. (10) ($r^2 = 0.98$; note that IP must be replaced with dimensions of $\mu\text{m}^2 \cdot \text{L} \cdot \text{min}^{-1}$).

$$DP_{\text{oral}}^{\text{in}} = 0.8737 [1 - \exp(-18.84 \times 10^{12} \times \text{IP})]. \quad (10)$$

Deposition probability in the oral cavity during exhalation is reported to be zero [20], therefore:

$$DP_{\text{oral}}^{\text{ex}} = 0. \quad (11)$$

5.3. Deposition within bronchial tree

The following common-used deposition formulas employed for calculation of the deposition probability in the present work are recommended by NCRP [21]. These correlations are analytical equations based on mathematical modeling.

5.3.1. Deposition by diffusion

The following equation is utilized in this study to estimate the probability of deposition by diffusion:

$$p_d = 1 - 0.819e^{-14.63\Delta} - 0.0976e^{-89.22\Delta} - 0.0325e^{-228\Delta} - 0.0509e^{-125.9\Delta^{2/3}}, \quad (12)$$

where $\Delta = \pi \bar{D}L/4Q$ and \bar{D} is the particle diffusivity, L is the tube length and Q is the volumetric flow rate.

The probability of diffusion during a pause time t is:

$$p_d = 1 - \exp\left(-23.136 \frac{\bar{D}t}{D^2}\right), \quad (13)$$

where D is the tube diameter.

5.3.2. Deposition by inertial impaction

Deposition of the particles by inertial impaction is a factor of airway geometry and particle stokes number. In this model, the probability of deposition by impaction is computed by the following equations:

$$p_i = 1 - (2/\pi) \cos^{-1}(\beta \text{St}) + (1/\pi) \sin [2 \cos^{-1}(\beta \text{St})] \quad \text{for } \beta \text{St} < 1, \quad (14a)$$

$$p_i = 1 \quad \text{for } \beta \text{St} > 1, \quad (14b)$$

where β is the effective branching angle and $\text{St} = \rho_p d_p^2 U / (18\mu D)$ with U being the mean flow velocity.

Contrary to the previous investigations of Koblinger and Hofmann [4,16], Hofmann and Koblinger [5,6] and Zhang et al. [13], the branching

angle applied in Eqs. 14(a) and 14(b), in the current simulation, differs from the geometrical branching angle, which is calculated in the structure simulation. Effective branching angles suggested by Balashazy et al. [22] for minor and major daughters, are utilized in this model. For the minor daughter, the effective branching angle, ψ , could be determined using Eq. (15):

$$\psi = \frac{7.5\theta}{35} + 27.5, \quad (15)$$

where θ is the actual branching angle of the tube.

For the major daughter, Eq. (16) must be applied to calculate the effective branching angle χ :

$$\chi = \frac{D_{d1}^2}{D_d^2}(\psi - \theta) + \theta, \quad (16)$$

where θ is the actual branching angle of the tube, D_d is the diameter of the symmetrical daughter airway, $D_{d2} = (D_{d1}^2 + D_{d2}^2)/2$. D_{d1} is the diameter of the minor daughter and D_{d2} is the diameter of the major daughter ($D_{d1} < D_{d2}$).

5.3.3. Deposition by sedimentation

Particle deposition due to sedimentation can be estimated using the following equation:

$$p_s = 1 - \exp\left(\frac{4}{\pi} \frac{\nu_{\text{settling}}}{U} \frac{L}{D} \cos\omega\right), \quad (17)$$

where ν_{settling} is the terminal settling velocity given as $\nu_{\text{settling}} = C_{\text{slip}} \rho_p g d_p^2 / (18\mu)$, with C_{slip} being the Cunningham slip correction factor and the subscript p refers to the properties of the particle. ω is the inclination angle relative to gravity $\omega = (\pi/2) - \varphi$, where φ is the gravity angle of the tube.

5.3.4. Total deposition

According to the simultaneous effect of deposition mechanisms, and assuming that the deposition mechanisms are mutually exclusive, the Goo and Kim [23] formula is applied to the current simulation for calculation of the total deposition probability:

$$p = p_d + p_i + p_s - p_d p_i - p_d p_s - p_i p_s + p_d p_i p_s. \quad (18)$$

5.4. Deposition within alveolated ducts

Along with the appearance of alveoli around the walls of pulmonary airways, deposition probability calculations differ from the calculation methods used in the bronchial tree. There are some uncertain input parameters involved in deposition simulations in the acinar region:

- (1) Whether the particle enters the sacs covering the tubes;
- (2) Whether the air carrying the particle mixes with the residual air of the alveoli;

- (3) Whether the particle exhales in the first exhalation.

In the present work, we used the probability distribution mentioned by Weibel et al. [15]. They assume that the walls of the pulmonary airways are covered by alveoli in the ratio of 0.2, 0.4 and 0.7 in the first three generations and 1 for the next 6 generations.

The next parameter associated with some uncertainty is the mixing factor. Mixing depends on breathing conditions and particle size. Unfortunately, such detailed information is currently unavailable. Several authors have analyzed mixing effects on particle deposition [24]. However, they have applied CFD techniques in a specified structure and their results are not applicable to our model. A constant mixing factor of 0.25, utilized by Hofmann and Koblinger [5], is used in this simulation.

The probability of exhalation after mixing in the acinus is equal to the ratio of the tidal and total lung volumes [5].

The correlations used for deposition calculation of the duct-shaped portion of the acinar pathways in this model are previously described in Section 4.3. Deposition in the alveolated portion is also estimated by the correlations recommended by Koblinger and Hofmann [16]. Total deposition probability in the acinar airway alveolus is calculated using the following correlation:

$$p_{alv} = p_s + p_d - p_s p_d, \quad (19)$$

where p_s and p_d are deposition probability by sedimentation and diffusion, respectively.

The total fraction of the particles deposited within each acinar pathway can be calculated using Correlation (20).

$$df_{alv} = df_{cyl} + df_{alv}, \quad (20)$$

where df_{cyl} and df_{alv} are deposited fractions on the cylindrical-shaped portion and in the alveoli, respectively.

6. Reference data set

In the current model, the following reference data set (Table 2) is utilized for the normal breathing condition, lung volume and inspiration airflow.

7. Results and discussion

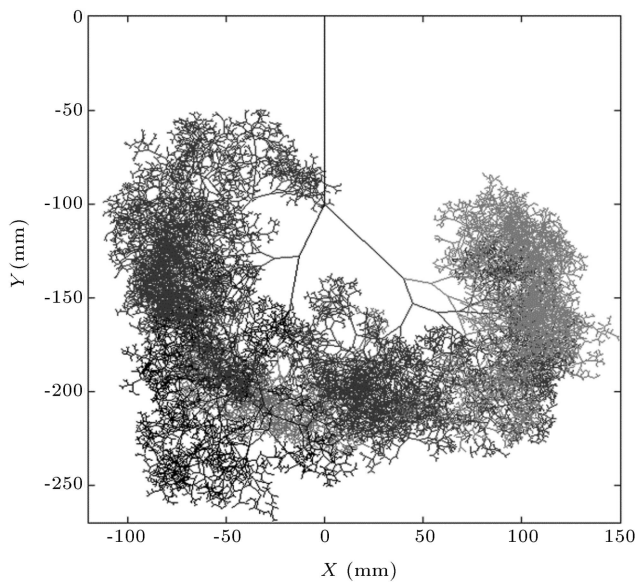
7.1. Lung structure

The structure of the simulated “whole lung” bronchial tree airways, using Raabe’s data base [2] for the first 5 generations, is illustrated in Figure 3. This structure satisfies lung morphometry adequately.

The mean values of the statistical lung structures simulated in this study are reported in Table 3. The

Table 2. Compilation of the reference data set.

Inhalation parameters	Value
Tidal volume	1000 cm ³
Total lung volume	3000 cm ³
Inspiration time	1.8 s
Expiration time	1.8 s
Breath-hold time	0.2 s
Air inhalation flux	500 cm ³ per breath
Inspiration frequency	20 times per minute
Air viscosity	2e – 5 Pa.s
Particles density	1 g.cm ⁻³

**Figure 3.** Whole lung tracheobronchial airways projected on the chest plane (first 5 generations are simulated using Raabe data base).

estimated total volume of acinar airways in this model is 5810 cc. This is in good agreement with total lung capacity, which is reported to be 5800 cc [25]. The total volume of the simulated statistical lung structures (5930 cc) is also in good agreement with the Weibel model (5850 cc). However, based on the stochastic nature of the simulated lung and the modifications made in termination phenomena and pulmonary airway structures, lobar volumes (which are mainly affected by the pulmonary airways) do not match the values reported by Yeh and Schum [14]. To solve this problem,

airway dimensions are multiplied to a scaling factor ranging from 0.7-1.3.

The total number of the bronchial tree airways grows continuously up to generations 15-16, where pulmonary airways start to appear. In this study, the average value of 2.8 is calculated for the length to diameter ratio (L/D). Additionally, the mean values of the bronchial tree airway generations and total lung generations are intended to be 15 and 25, respectively.

7.2. Airflow distribution

As the generation number increases, the number of the pathways grows and each pathway's share of the inhaled air drops rapidly. To facilitate the comparison between the method developed in this study and the one previously used by Koblinger and Hofmann, the following correlation is considered:

$$\frac{f_1}{f_2} = \left(\frac{d_1}{d_2}\right)^x, \quad (21)$$

where f_1 and f_2 are the 1st and the 2nd daughters' flux fraction of their parent and d_1 and d_2 are the daughters' diameters, respectively.

Koblinger and Hofmann [16] computed each daughter's flux share of its parent according to the ratio of daughter cross sections. This means that the value of x in their model is equal to 2. They have suggested this value based on a simplified geometry consisting of a tube (parent) divided into two tubes (daughters). Consequently, downstream pathways are not considered when utilizing this value.

As described in Section 4, in this model, inspiratory flow is divided among lung pathways based on the expansion/contraction of the pulmonary airways and in an upward manner, starting from respiratory sacs and continuing toward the trachea. In the current simulation, $x = 2.5$ has the most occurrence probability (median); however, the weighted average (mean) of this distribution is 3.15. This clearly shows that, based on this developed model in which all pathways are considered, the commonly used $x = 2$ is erroneous for use.

7.3. Depth of penetration into the lung

In a given breathing cycle, not all particles entering the trachea at the beginning of the inhalation have enough time to reach deep into the respiratory airways. Geometrical distribution of the airways and inhaled air flux are two of the main factors affecting the

Table 3. Lung structure simulation results.

	RU	RM	RL	LU	LL	Whole lung
Total number of the TB airways	10200	4700	9900	8900	11600	45300
Total number of the acinar packs	9000	2300	4600	7600	7600	31100
Total number of the acinar airways	4023000	1028100	2056200	3397200	3397200	13901700

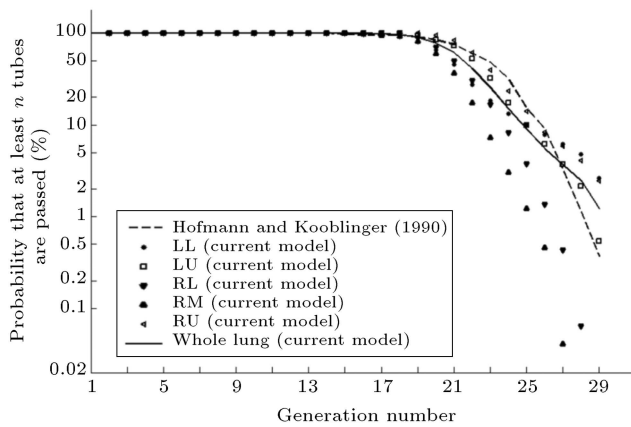


Figure 4. Complementary cumulative distributions of airways passed with the assumption of no deposition.

depth of penetration of particles into the lung airways. Cumulative distributions of airways passed, with the assumption of no deposition, are illustrated in Figure 4 for individual lobes and the whole lung.

According to Figure 4, the number of the pulmonary pathways which could be passed by the particles decreases as the generation number increases, i.e. only 1% of the particles could reach the 29th generation. However, deposition may stop particles before they reach this theoretical depth.

Results obtained in this study are compared with the results reported by Hofmann and Koblinger [5] and the agreement is satisfactory.

7.4. Deposition fractions

The results based on the reference data set given in Section 6 are presented in this section. It is noteworthy that the Monte Carlo results are always associated with a statistical uncertainty. However, this uncertainty decreases as the number of considered pathways in the “whole lung” model grows.

In this study, whole lung pathways are considered and regional deposition is calculated in each of these airways. These deposition fractions could be displayed for each individual pathway in a 3D figure. In order to shorten the paper, some of the main calculated distributions are presented here.

7.4.1. Total deposition

Total deposition in the “whole lung” is calculated during a full breathing cycle for 39 different monodisperse particles, with various diameters ranging from 0.01 to 10 microns. In this section, the inhalation period is assumed to be 2 seconds. In Figure 5, simulation results of the deposited fraction versus particle diameter are displayed for the bronchial tree, acinar and total lung airways. As seen in this figure, for relatively small particle diameters, the deposited fraction of the particles decreases as the particle diameters increase. However, for large particle diameters, the deposited

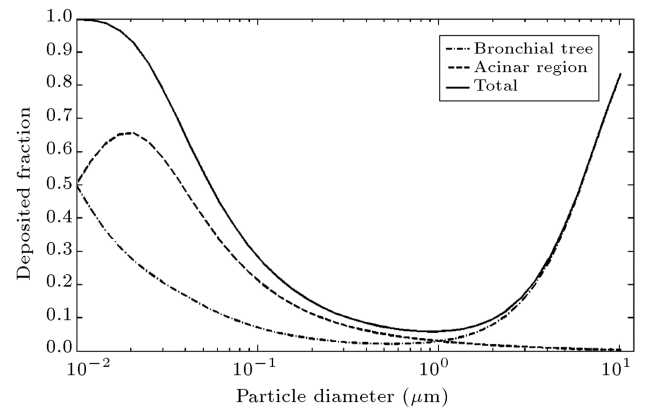


Figure 5. Total deposition vs. particle diameter.

fraction increases as particle diameter grows. When the particles are relatively small, diffusion is dominant in both the bronchial tree and acinar airways. As the particle diameter increases, deposition due to diffusion is reduced and sedimentation and impaction become dominant. As a result, particles with diameters between 0.4 to 0.7 μm have the minimum deposited fraction in the lung airways. These particles are big enough to have a minor diffusion, but are too small to have significant sedimentation and impaction. As a result, none of the triple deposition mechanisms is dominant for this range of particle diameter.

When the particle size exceeds this range, impaction and sedimentation become significant in lung pathways. As the deposition in bronchial tree pathways increases, the statistical weight of the particles entering acinar airways decreases. Consequently, the weight of the particles deposited in this region decreases. However, deposition probability still increases in these airways.

In the pulmonary region, there is a peak in the curve of deposited fraction versus particle diameter when the particle diameter increases from 0.01 to 2 μm . In this range of particle sizes, as particle diameter increases, deposition decreases in the tracheobronchial, and the statistical weight of the particles entering the pulmonary airways increases. Sedimentation also increases in pulmonary airways while diffusion weakens slightly. As a result, deposition increases in this range of particle sizes. When the particles grow further in size, diffusion decreases greatly and deposition diminishes.

In Figure 6, simulation results of the total deposited fraction during a full breathing cycle, considering nasal breathing, are compared with the experimental data reported by Schiller et al. [26], Heyder et al. [27], Foor et al. [28], Melandr et al. [29], and Tu and Knutson [30]. The simulation results in this figure are obtained for a full breathing cycle of 4 s.

The simulation results are in good agreement with experimental data for particles with diameters

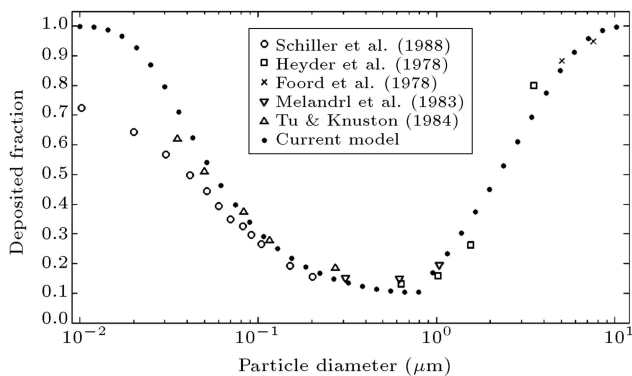


Figure 6. Comparison of the simulation results for total deposition vs. particle diameter with experimental results reported by Hofmann and Koblinger [5].

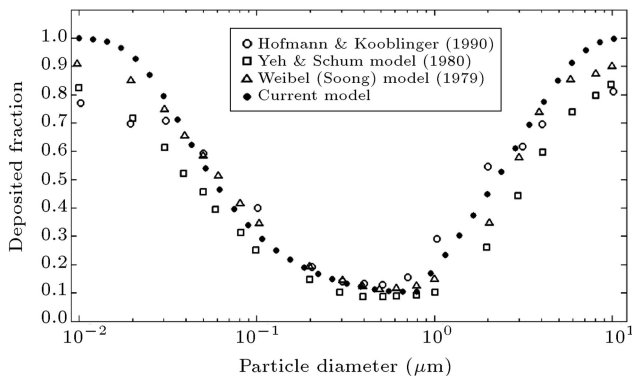


Figure 7. Comparison of the total deposition vs. particle diameter in the current model with the previous models of Hofmann and Koblinger [5].

larger than $1\mu\text{m}$ (Figure 6). The probability of particle deposition by diffusion increases as the particles and the airways dimensions become smaller. As a result, these particles mainly deposit in the pulmonary airways. However, these small airways cannot be considered accurately in experimental investigations and the reported deposition fractions may differ with the simulation results. The greater difference between the simulation and experimental results for smaller particles supports this justification.

In Figure 7, deposition results of a full nasal breathing cycle are compared with other theoretical models. Calculations with the deterministic symmetric models of Weibel [1] and Yeh and Schum [14] were carried out by Hofmann and Koblinger [5]. A full breathing cycle of 4 s is assumed in all these deterministic models. They have also considered oronasal breathing deposition. Taking into account these variations, the shapes of the deposition curves are, in general, similar to each other. Comparing this figure with Figure 6, it can be concluded that the differences between the current simulation results and the experimental results are much smaller than those of other theoretical predictions.

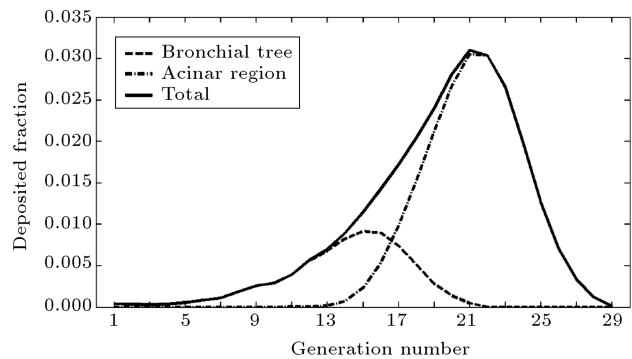


Figure 8. Regional deposited fraction of $0.1\mu\text{m}$ particles in bronchial tree, acinar and total lung airways.

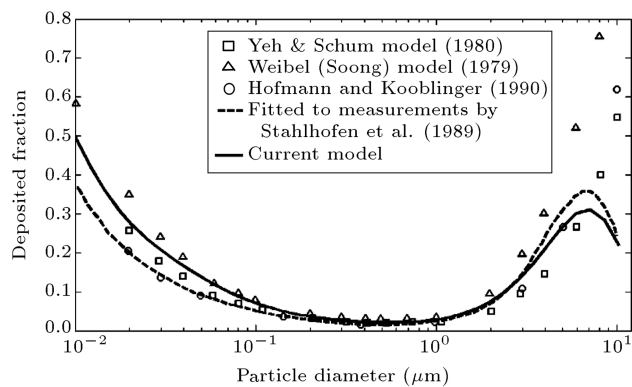


Figure 9. Fraction of inhaled particles deposited in the tracheobronchial region. Comparison of results calculated in current simulation with other models reported by Hofmann and Koblinger [5].

The small difference between simulation results and the models illustrated in Figure 7 for small and big particles can be due to the variation in pulmonary airway structure, termination assumption, flux distribution calculation methods, and, mainly, to the variation in applied deposition formulas (in the nasal cavity).

7.4.2. Regional deposition

The regional deposited fraction of $0.1\mu\text{m}$ particles for the bronchial tree, acinar and total lung, is illustrated in Figure 8. It can be seen that the deposited fraction of these particles is maximum in generation 15, where the total number of the bronchial airways is maximum. While the generation number increases further, acinar packs appear and the total number of pulmonary airways increases. According to this figure, the deposited fraction of $0.1\mu\text{m}$ particles is maximum in the range of 21–23th generations.

The deposited fraction of particles in the bronchial tree region is illustrated in Figure 9. Current simulation results are compared with experimental data reported by Stahlhofen et al. [18], the results reported by Hofmann and Koblinger [5], and other theoretical predictions based on the modified models

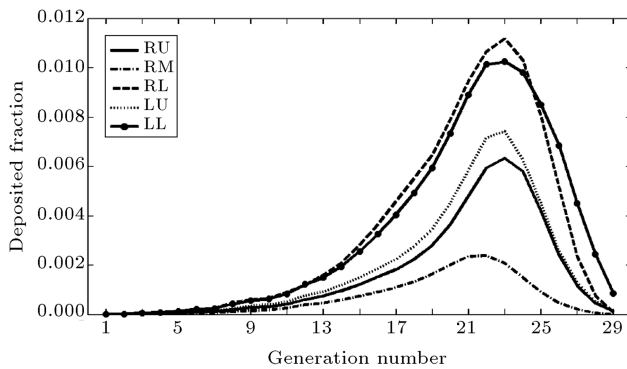


Figure 10. Regional deposited fraction of $0.1 \mu\text{m}$ particles in each lung lobe.

Table 4. Lobar deposition fractions of $0.1 \mu\text{m}$ particles.

Lobe	Relative deposition fraction (%)				
	RU	RM	RL	LU	LL
Current model	15.0	6.3	30.3	17.7	30.7
Hofmann and Koblinger [5]	12.0	5.6	33.8	15.9	33.3

of Weibel [31] and Yeh and Schum [14], reported in Hofmann and Koblinger [5] for the bronchial tree region. As can be seen, contrary to other theoretical predictions, the current model results are in good agreement with experimental results.

For larger particle diameters, a considerable fraction of particles is deposited in the nasal cavity. Therefore, the statistical weight of the particles delivered to the bronchial tree airways is less than that of the smaller particles. As a result, the deposited fraction of these large particles is decreased.

The regional deposited fraction of $0.1 \mu\text{m}$ particles is illustrated in Figure 10 for each of the lung's five lobes. Comparing these curves with the data reported by Yeh and Schum [14] for lobar volumes, it can be concluded that while the lobe volumes grow, the deposited fraction of particles in these respiratory volumes increases.

For this case, the relative total deposition fractions in each of the lung lobes are also presented in Table 4. Considering the modification applied to the process of the simulation of lung airways, airflow distribution and deposition correlations, these results are in good agreement with the values reported by Hofmann and Koblinger [16].

8. Conclusions

Results obtained by this model show satisfactory agreement with the “single path” modeling over a wide range of particle diameters. In comparison, deterministic models involve more simplifications of the lung's morphometry than the current model, which simulates

a statistical stochastic “whole lung”. The corrections applied to the stochastic lung modeling algorithm provided by Hoffman and Koblinger [5] assisted in construction of the whole lung instead of a series of single paths or a collection of a few bifurcations. Consequently, this model provides an improved lung model, in which all pathways are taken into account at the same time. Moreover, in the present work, all lung pathway spatial coordinates are calculated and their obstruction could be modeled in ongoing investigations. This model provides information on the amount of particles deposited in each lung pathway and at each spatial location (e.g. at $(x, y) = (-100 \text{ mm}, -70 \text{ mm})$ or in the 7th generation in lower left lobe). However, previous models only provide information on the average deposition in different generations or lobes of the lung.

The changes made in termination correlation and the scheme used in calculation of the airflow distribution among lung pathways result in a more realistic approximation of lung morphology.

While statistical lung modeling has the advantage of a more realistic description of lung morphometry, this level of superiority requires supplementary information of simulation parameters. As a result, the present study requires further refinement. The current simulation program is intended to facilitate such improvements.

References

1. Weibel, E.R., *Morphometry of the Human Lung*, Academic Press, New York (1963).
2. Raabe, O.G., Yeh, H.C., Schum, G.M. and Phalen, R.F. “Tracheobronchial geometry human: human, dog, rat, hamster”, LF-53 Lovelace Foundation Report, Albuquerque, New Mexico, USA (1976).
3. Horsfield, K., Dart, G., Olson, D.E., Filley, G.F. and Cumming, G. “Models of the human bronchial tree”, *J. of Applied Physiology*, **31**, pp. 207-217 (1971).
4. Koblinger, L. and Hofmann, W. “Analysis of human lung morphometric data for stochastic aerosol deposition”, *J. of Physics in Medicine and Biology*, **30**(6), pp. 541-556 (1985).
5. Hofmann, W. and Koblinger, L. “Monte Carlo modeling of aerosol deposition in human lungs. Part II: deposition fractions and their sensitivity to parameter variations”, *J. of Aerosol Science*, **21**(5), pp. 675-688 (1990).
6. Hofmann, W. and Koblinger, L. “Monte Carlo modeling of aerosol deposition in human lungs. Part III: Comparison with experimental data”, *J. of Aerosol Science*, **23**(1), pp. 51-63 (1992).
7. Asgharian, B., Price, O.T. and Hofmann W. “Prediction of particle deposition in the human lung using

- realistic models of lung ventilation”, *J. of Aerosol Science*, **37**(10), pp. 1209-1221 (2006).
8. Des Jardins, T., *Cardiopulmonary Anatomy & Physiology; Essentials for Respiratory Care*, 4th Edn., Delmar (a division of Thomson Learning, Inc.), ISBN 0-7668-2533-7 (2002).
 9. West, J.B., *Respiratory Physiology: The Essentials*, 9th Edn., Wolters Kluwer Health Publication (2012).
 10. Balashazy, I. and Hofmann, W. “Particle deposition in airway bifurcations— I. Inspiratory flow”, *J. of Aerosol Science*, **24**(6), pp. 745-772 (1993).
 11. Heistracher, T. and Hofmann, W. “Physiologically realistic models of bronchial airway bifurcations”, *J. of Aerosol Science*, **26**(3), pp. 497-509 (1995).
 12. Su, W.C. and Cheng, Y.S. “Deposition of fiber in human airway replica”, *J. of Aerosol Science*, **37**(11), pp. 1429-1444 (2006).
 13. Zhang, Z., Kleinstreuer, C. and Kim, C.S. “Comparison of analytical and CFD models with regard to micron particle deposition in a human 16-generation tracheobronchial airway model”, *J. of Aerosol Science*, **40**(1), pp. 16-28 (2009).
 14. Yeh, H.C. and Schum, G.M. “Models of human lung airways and their application to inhaled particle deposition”, *Bulletin of Mathematical Biology*, **42**(3), pp. 461-480 (1980).
 15. Weibel, E.R., Sapoval, B. and Filoche, M. “Design of peripheral airways for efficient gas exchange”, *J. of Respiratory Physiology and Neurobiology*, **148**(1), pp. 3-21 (2005).
 16. Koblinger, L. and Hofmann, W. “Monte Carlo modeling of aerosol deposition in human lungs. Part I: Simulation of particle transport in a stochastic lung structure”, *J. of Aerosol Science*, **21**(5), pp. 661-674 (1990).
 17. Shi, H., Kleinstreuer, C. and Zhang, Z. “Modeling of inertial particle transport and deposition in human nasal cavities with wall roughness”, *J. of Aerosol Science*, **38**(4), pp. 398-419 (2007).
 18. Stahlhofen, W., Rudolf, G. and James, A.C. “Intercomparison of experimental regional aerosol deposition data”, *J. of Aerosol Medicine and Pulmonary Drug Delivery*, **2**(3), pp. 285-308 (1989).
 19. Zhang, Z., Kleinstreuer, C. and Kim, C.S. “Micro-particle transport and deposition in a human oral airway model”, *J. of Aerosol Science*, **33**(12), pp. 1635-1652 (2002).
 20. Yu, C.P., Diu, C.K. and Soong, T. “Statistical analysis of aerosol deposition in nose and mouth”, *American Industrial Hygiene Association Journal*, **42**(10), pp. 726-733 (1981).
 21. NCRP “Deposition, retention, and dosimetry of inhaled radio active substances”, Report no. 125, National Council on Radiation Protection and Measurements, Bethesda, MD, USA (1997).
 22. Balashazy, I., Hofmann, W. and Martonen, T.S. “Inspiratory particle deposition in airway bifurcation models”, *J. of Aerosol Science*, **22**(1), pp. 15-30 (1990).
 23. Goo, J. and Kim, C.S. “Theoretical analysis of particle deposition in human lungs considering stochastic variations of airway morphology”, *J. of Aerosol Science*, **34**(5), pp. 585-206 (2003).
 24. Haber, S., Yitzhak, D. and Tsuda, A. “Gravitational deposition in a rhythmically expanding and contracting alveolus”, *J. of Applied Physiology*, **95**(2), pp. 657-671 (2003).
 25. Guyton, C. and Hall, J.E., *Textbook of Medical Physiology*, 11th Edn., Elsevier Inc., International Edition ISBN 0-8089-2317-X (2006).
 26. Schiller, Ch.F., Gebhart, J., Heyder, J., Rudolf, G. and Stahlhofen, W. “Deposition of monodisperse insoluble aerosol particles in the 0.005 to 0.2 μm size range within the human respiratory tract”, *Annals of Occupational Hygiene* **32**, inhaled particles VI, pp. 41-49 (1988).
 27. Heyder, J., Gebhart, J., Roth, C., Stahlhofen, W., Stuck, B., Tarroni, G., De Zaiacomo, T., Formignani, M., Melandri, C. and Prodi, V. “Intercomparison of lung deposition data for aerosol particles”, *J. of Aerosol Science*, **9**(2), pp. 147-155 (1978).
 28. Foord, N., Black, A. and Walsh, M. “Regional deposition of 2.5 – 7.5 μm diameter inhaled particles in healthy, male non-smokers”, *J. of Aerosol Science*, **9**(4), pp. 343-357 (1978).
 29. Melandri, C., Tarroni, G., Prodi, V., De Zaiacomo, T., Formignani, M. and Lombardi, C.C. “Deposition of charged particles in the human airways”, *J. of Aerosol Science*, **14**(5), pp. 657-669 (1983).
 30. Tu, K.W. and Knutson, E.O. “Total deposition of ultrafine hydrophobic and hygroscopic aerosols in the human respiratory system”, *J. of Aerosol Science and Technology*, **3**(4), pp. 453-465 (1984).
 31. Soong, T.T., Nicolaidis, P., Yu, C.P. and Soong, S.C. “A statistical description of the human tracheobronchial tree geometry”, *Respiration Physiology*, **37**(2), pp. 161-172 (1979).

Biographies

Ramin Dastanpour obtained BS and MS degrees from Isfahan University of Technology Isfahan, Iran, and is currently a PhD degree student of Mechanical Engineering at the University of British Columbia (UBC), Canada. His research interests include simulation of respiratory systems, particle transport and CFD simulations.

Mojdeh Monjezi obtained BS and MS degrees from Isfahan University of Technology, Isfahan, Iran, and

is currently a PhD degree candidate at the Center of Excellence in Energy Conversion, School of Mechanical Engineering, Sharif University of Technology (SUT), Tehran, Iran. Her research interests include biofluids, modeling of particle transport and respiratory systems and aerosol dynamics.

Mohammad Said Saidi is Professor of Mechanical Engineering at Sharif University of Technology, Tehran, Iran. His research interests include modeling and numerical analysis of transport and deposition

of aerosol particles, modeling and numerical analysis of biofluids, modeling and numerical analysis of thermal-hydraulics of porous media and micro channels.

Ahmad Reza Pischevar is Professor of Mechanical Engineering at Isfahan University of Technology, Isfahan, Iran, and is Editor-in-Chief of the Journal of Computational Methods in Engineering. His research interests include compressible unsteady flow, multi phase flows and CFD Simulations.